Considering the interaction of switch and stock rails in modelling vehicle-track interaction in a switch panel diverging route

Michel Sebes, Yann Bezin

Taylor & Francis
Taylor & Francis Group

Vehicle System Dynamics
International Journal of Vehicle Mechanics and Mobility

ISSN: (Print) (Online) Journal homepage: https://www.tandfonline.com/loi/nvsd20

Considering the interaction of switch and stock rails in modelling vehicle-track interaction in a switch panel diverging route

M. Sebès & Y. Bezin

To cite this article: M. Sebès & Y. Bezin (2021): Considering the interaction of switch and stock rails in modelling vehicle-track interaction in a switch panel diverging route, Vehicle System Dynamics, DOI: 10.1080/00423114.2021.1947510

To link to this article: https://doi.org/10.1080/00423114.2021.1947510

Published online: 30 Jun 2021.

VEHICLE SYSTEM DYNAMICS
https://doi.org/10.1080/00423114.2021.1947510

Considering the interaction of switch and stock rails in modelling vehicle-track interaction in a switch panel diverging route

M. Sebès[a] and Y. Bezin [b]

[a]COSYS-GRETTIA, Univ Gustave Eiffel, IFSTTAR, Marne-la-Vallée, France; [b]Institute of Railway Research, University of Huddersfield, Huddersfield, UK

ABSTRACT

Vehicle-track interaction in a switch panel diverging route is studied with a focus on the way its components may interact in the lateral direction. Taking one of the cases of S&C benchmark as the base model, several variants of the co-running track model are considered. In the first series of simulation, the effect of the lateral separation of the switch rail and stock rail is investigated, showing that only small differences are found in terms of wheel/rail forces between a track model where both rails are coupled, and one where they are free to move with respect to one another. Only transient effects are visible at the beginning and at the end of the two-point contact on both rails. While small, these differences can have some influence in terms of rolling contact fatigue and wear prediction. In the second series of simulation, co-running track models are developed including the baseplate and taking into account such effects as switch rail/stock rail contact at the undercut plane and dry friction. Significant changes are observed in the load distribution within the switch panel. Conclusions should be consolidated through experimental field measurement and using more realistic track models, e.g. discretely supported rail beam models.

ARTICLE HISTORY
Received 2 February 2021
Revised 8 June 2021
Accepted 20 June 2021

KEYWORDS
Switch and crossings; railway dynamics; wheel-rail contact; vehicle-track interaction; track models; switch rails; stock rails

1. Introduction

In a railway track, a switch panel is a complex mechanical system composed of several components: switch rails, stock rails, sliding or baseplate, stock rails and baseplate pads, etc. While considering the passage of a train, the dynamic interactions between the loading wheels and all of these components is a complex problem that has rarely been studied in detail, especially in the diverging route of a turnout.

When modelling switches using multibody dynamics software, it is common practice to model the switch and stock rails as a single element (i.e. rigid body or degree of freedom-*dof*) with an associated single rigid profile. This *dof* body is attached through a resilient element to either a third mass representing the sleeper layer or directly to the ground. In practice, this representation is not realistic. The switch rail typically rests directly on a baseplate attached to the sleeper, while the stock rail is connected to the baseplate via

CONTACT M. Sebès michel.sebes@univ-eiffel.fr

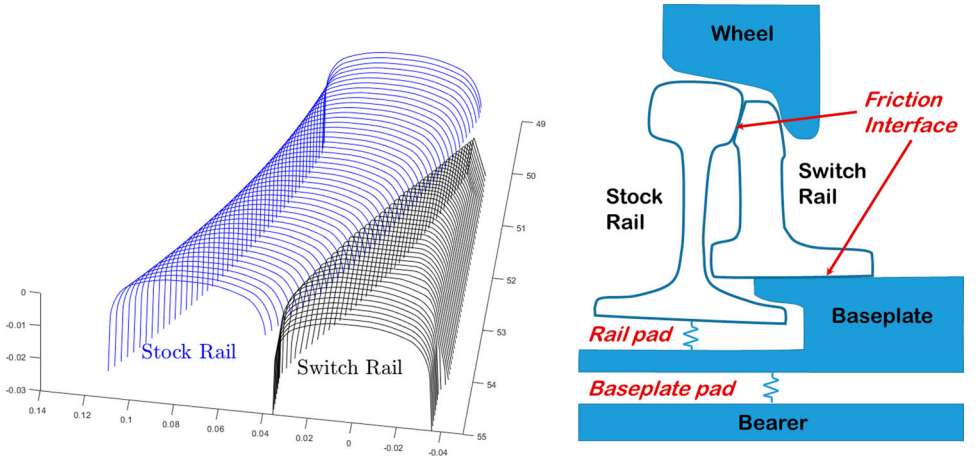

Figure 1. Separation of switch-stock rails. GB CEN56 switch and stock profiles (left). Representative of ideal track schematic representing the specific switch panel configuration (right).

a resilient layer, as shown in Figure 1. However, commercial Multibody Dynamics (MBS) software does not readily offer such a track model and the most obvious solution to separate the switch and stock rail is to use the capability they have to model additional wheel contact with a guide or stock rail. This usually allows the user to define another set of possible contact with a fourth and fifth rail body in the track (one on either side potentially). It is to be noted that the separation of the two rails has recently received some interest from the scientific community [12] accounting only for the vertical interaction and not taking into account the vehicle or track dynamics, while a dynamic study was presented in [3].

The purpose of this paper is twofold:

- The first part concerns the separation of rails in the lateral direction in the wheel/rail (W/R) contact. The goal is to evaluate the necessity at the contact level to take into account the relative lateral *dof* of the switch rail with respect to the stock rail, which was not considered in [3].
- The second objective is to elaborate more detailed track models of the switch panel including the baseplate, to assess their influence on W/R forces, and also on forces between the components of the switch panel.

The GB 56 kg rail diverging switch case [45] (Run #2 of the S&C benchmark [6]) is considered as the case study in the present paper. Implementations are done in Multibody Systems (MBS) software VI-Rail and VOCO.

The base model for the track is the so-called 'co-running' track model as defined in the S&C benchmark. In this model, the switch and the stock rails are connected to a sleeper-track mass but they are disconnected from one another in the lateral direction. This assumption may lead to unrealistic results in the diverged route where a contact on the mating face of the two components is likely between the stock rail and the switch rail. A variant of the benchmark track model is therefore considered where the switch rail and the stock rail are coupled along the lateral direction. Comparing this model with the initial

model allows a qualitative assessment of the effect of the separation of rails in the lateral direction.

In the second part of the paper, varying track models introducing a baseplate are considered. Different variants are considered to study the following effects:

- steel on steel contact between stock rail and switch rail;
- dry friction between baseplate and switch rail;
- dry friction between stock rail and switch rail.

2. Methodology

2.1. Case study

Run #2 of the benchmark (GB 56 diverging switch case) is chosen as a case study. The reader may refer to a thorough description of the settings in the benchmark statement [6].

The only modification in the VOCO settings concerns the output sampling frequency, which has been increased to 10 kHz instead of 2 kHz initially. This is due to the introduction of a small mass (baseplate) and high stiffness (contact) in some of the configurations.

MBS software VI-Rail and VOCO are used to address the case study. Simple non-Hertzian contact models are implemented in both software packages. VI-Rail uses the Kik–Piotrowski method [7] for normal contact and FASTSIM [8] for tangential contact. The STRIPES method [9] is considered in VOCO in order to handle the normal and tangential contact. In this study linear stiffness (500 kN/mm) and damping (20 N·s/mm) are introduced in VOCO at the W/R contact level. A Hertzian stiffness with standard steel properties is considered in VI-Rail with a Hertzian damping ratio of 0.001 [10]. The reader may refer to the summary of the method statements [11], to the individual online method statements of each MBS package [12], and finally to the paper dedicated to W/R contact written in the frame of this special issue [13], for a thorough description of the W/R contact methods used by each software.

2.2. Track models configuration

Results with the track model of the benchmark are used as a reference. This is a co-running model with constant properties along the track. Its parameter values are kept unchanged unless explicitly stated.

In the benchmark (Figure 2), no link exists between the stock rail and the switch rail. In the diverged route, this assumption may lead to some unrealistic results at the flanging wheel of the leading wheelset, where the lateral W/R forces acting on each component force the two rails together: the lateral force Y_{sw} acting on the switch rail is dominated by the flange contact normal component, while the force Y_{st} acting on the stock rail is mainly due to the thread contact tangential component and is acting in the opposite direction (Figure 3).

In order to assess the effect of the separation of rails in the lateral direction on W/R forces, a configuration is studied where lateral *dofs* of the switch rail and the stock rail (respectively $u_{y,sw}$ and $u_{y,st}$ in Figure 3) are coupled in the track model. In both VOCO

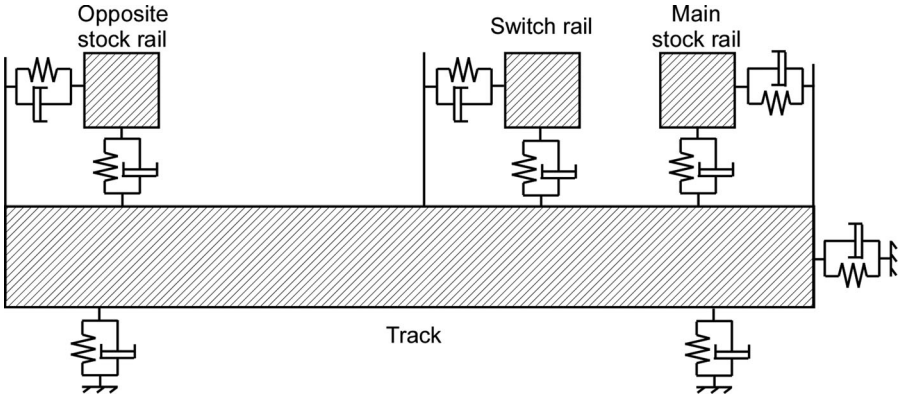

Figure 2. Co-running track model of the switch panel used for the benchmark.

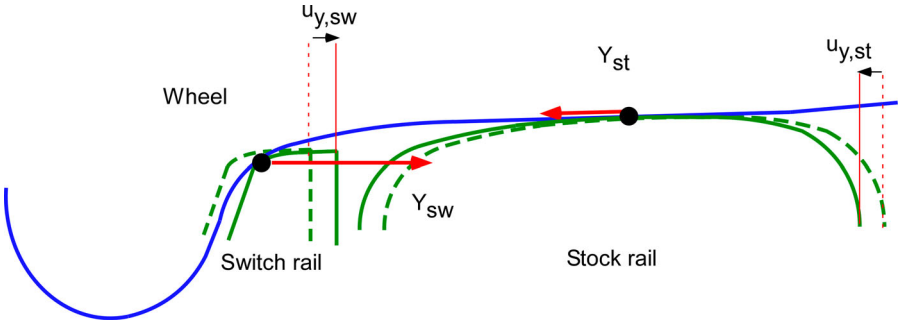

Figure 3. Sketch of lateral W/R forces acting on the switch rail and the stock rail.

and VI-Rail simulations, this coupling is replaced by a spring with a high stiffness of 15 MN/mm and damping 10 Ns/mm.

Next, a series of track models (Figure 4) is studied where a baseplate is introduced in the software VOCO. The baseplate is modelled as a mass, linked to the track through a baseplate pad. The switch rail rests on the baseplate with steel on steel contact. Model (a) is the simplest one where the baseplate is connected to the switch rail through stiff springs accounting for the steel on steel contact. In model (b), a unilateral contact is added at the undercut plane of angle ϕ between the switch rail and the stock rail. No initial gap is considered between the rails. In model (c), the lateral spring is removed at the interface between the baseplate and the switch rail, and is replaced by dry friction with a Coulomb's limit. The maximum lateral force is the vertical force times a constant friction coefficient. The same joint has been used in a study of the lateral resistance of the track with a flexible track model [14]. The model of the dry friction element is briefly described in [15]. The more elaborate model (d) takes into account dry friction with a Coulomb's limit between the switch rail and the stock rail. The maximum tangent force is the normal force times a constant friction coefficient. Model's topology is presented in Figure 4 and their parameter values are listed in Table 1. It is to be noted that some parameter values of Table 1 may not correspond to the actual design of the CEN56 switch panel, as they were not at the

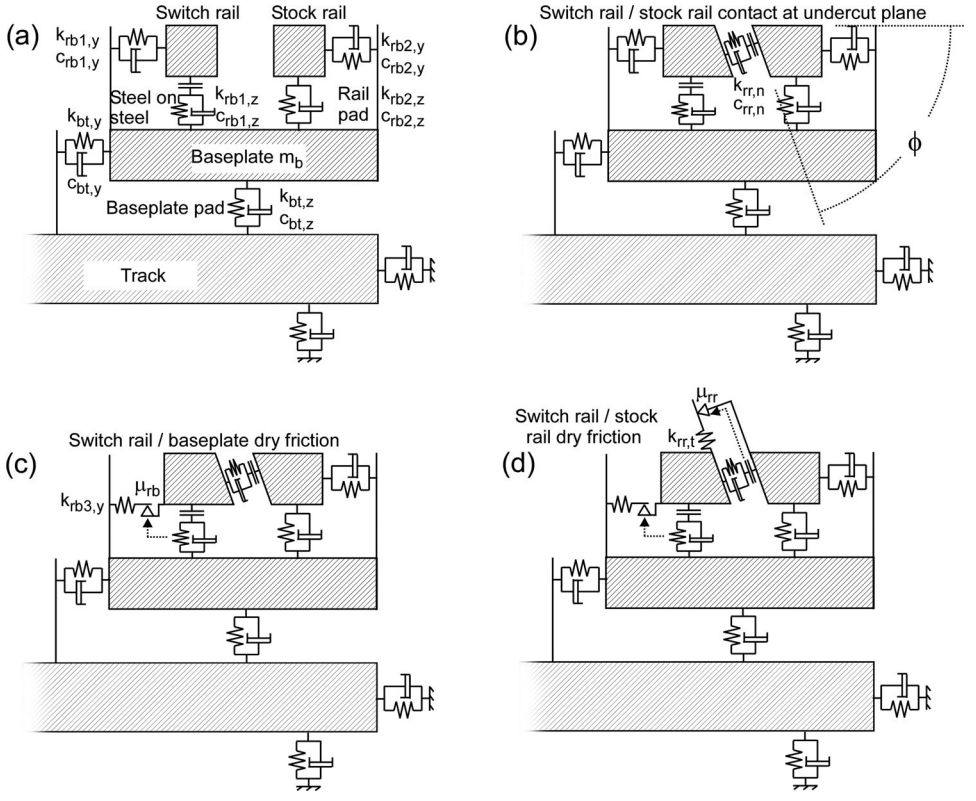

Figure 4. Topology of the track models (a), (b), (c) and (d).

disposal of the authors. Although the orders of magnitude of the input data are believed to be relevant, the validation of the presented results should be supported by actual physical measurements. It should also be noted that constant properties are used along the track. In the actual design (GB CEN56 CV type, 245 m radius), the moveable length of the switch rails for which the baseplates might be considered active is located approximately between 0 and 8.9 m with respect to the beginning of the switch, and the length over which the switch rail can contact the stock rail is about 4 m.

All results are plotted according to the conventions and coordinate systems of the benchmark:

- Y-axis points to the right, Z-axis points downward.
- W/R forces are given as applied on the rail.

Results are always considered at the flanging wheel of the leading wheelset as it is the one applying the highest lateral load on the switch-stock rail elements. As part of this study the authors also looked at the behaviour of the trailing axle of the front bogie, but the lateral forces applied were very low and no relevant differences were identified between the two modelling approaches (benchmark reference and direct connection).

Table 1. Parameter values of track models (a), (b), (c) and (d). Stiffnesses (k) are given in kN/mm, damping coefficients (c) in Ns/mm, masses (m) in kg.

Parameter	Track model	Description	Value
m_b	(a) (b) (c) (d)	Baseplate mass	40
$k_{rb2,z}$	(a) (b) (c) (d)	Stock rail pad vertical stiffness	150
$c_{rb2,z}$	(a) (b) (c) (d)	Stock rail pad vertical damping	100
$k_{rb2,y}$	(a) (b) (c) (d)	Stock rail pad lateral stiffness	30
$c_{rb2,y}$	(a) (b) (c) (d)	Stock rail pad lateral damping	150
$k_{bt,z}$	(a) (b) (c) (d)	Baseplate pad vertical stiffness	150
$c_{bt,z}$	(a) (b) (c) (d)	Baseplate pad vertical damping	100
$k_{bt,y}$	(a) (b) (c) (d)	Baseplate pad lateral stiffness	30
$c_{bt,y}$	(a) (b) (c) (d)	Baseplate pad lateral damping	150
$k_{rb1,z}$	(a) (b) (c) (d)	Switch rail/baseplate vertical stiffness	15000
$c_{rb1,z}$	(a) (b) (c) (d)	Switch rail/baseplate vertical damping	100
$k_{rb1,y}$	(a) (b)	Switch rail/baseplate lateral stiffness	1500
$k_{rb1,y}$	(a) (b)	Switch rail/baseplate lateral damping	100
ϕ	(b) (c) (d)	Undercut plane angle	70
$k_{rr,n}$	(b) (c) (d)	Stock rail/switch rail normal stiffness	1500
$c_{rr,n}$	(b) (c) (d)	Stock rail/switch rail normal damping	10
μ_{rb}	(c) (d)	Switch rail/baseplate friction coefficient	0.7
$k_{rb3,y}$	(c) (d)	Switch rail/baseplate lateral series stiffness	1500
μ_{rr}	(d)	Stock rail/switch rail friction coefficient	0.7
$k_{rr,t}$	(d)	Stock rail/switch rail tangent series stiffness	150

3. Results

3.1. Study of the separation of rails in the lateral direction

The track model of the benchmark does not consider any direct connection in the lateral direction between the stock rail and the switch rail. In a first approach, the benchmark model is modified by incorporating a rigid connection in the lateral direction between both rails. The comparison of this new model with the initial one allows to assess the effect on the contact conditions of the separation of rails in the lateral direction.

Figure 5 shows the comparison between the benchmark model (dotted lines) and the new one (solid lines) in terms of W/R contact forces for VOCO (blue) and VI-Rail (black). Plots on the left present results along the entire switch panel (1–6 m, zero being the start of the switch). Plots on the right focus in the zone where initial contact between the wheel flange and the switch rail occurs ($\sim$ 1.8 m). A sustained two-point contact occurs for nearly 2 m (distance 1.8–3.5 m) where the switch rail and the stock rail are forced together by lateral forces acting in opposite directions on both rail parts, and where relatively high longitudinal forces are acting in opposite direction on both rail parts (higher on the switch rail and pushing backwards). Beyond the two-point contact, there is departure from the stock rail, i.e. a full transfer of contact on the switch rail, characterised by a slightly reduced curving force (Y), reduced steering force (X), and increased centrifugal vertical force (Q) on the outer rail. Note that VOCO at that point shows a higher transient dynamic Q force of about 18 kN peak to peak amplitude ($\sim$ +/−15% of nominal load). VI-Rail on the other hand shows a few spikes on the Y and X forces.

These small differences can be seen from either software implementation due to their core differences and contact algorithm. They are discussed in the benchmark exercise independently from this paper. Instead, this paper focuses on the potential differences that may be observed by implementing a direct connection between the two rails. Regarding this

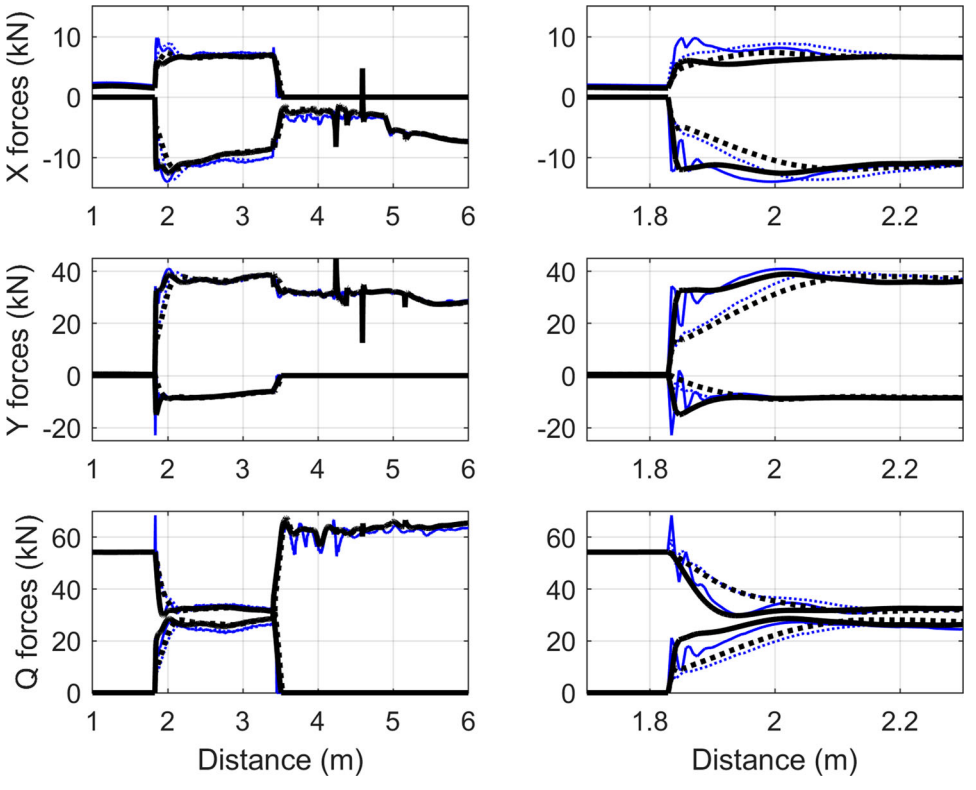

Figure 5. Run #2. Comparison of W/R contact forces between the track model of the benchmark (dotted line) and with an additional rigid connection in the lateral direction between both rails (solid line) for VOCO (blue) and VI-Rail (black). Zooming on the first load transfer on the switch rail in the right-hand side plots.

matter, both MBS codes do not predict significant changes caused by the connection. Only a local increase in forces is observed principally due to the switch rail making harder initial contact as it does not move laterally as much as it does in the benchmark definition. It may be noted these differences are not due to changes in contact conditions which would be caused by the rigid lateral connection. For instance, contact angles (not plotted) are almost the same in both models showing a similar flange contact at the outer wheel of the leading axle.

As the rise of forces going through flange contact is sharper in the case where lateral *dofs* are coupled, and although very localised, it is interesting to look at the difference this may have on rolling contact fatigue and wear prediction for the thinner part of the switch blade. Figure 6 shows the wear index (or T gamma [16]) in the area of first contact with the switch (left) and on full contact departure onto the switch rail (right). Another model is added to the comparison by fully constraining switch and stock rail in both vertical and lateral directions. Both constrained models show the increased wear damage on the initial flange contact, compared to the more forgiving benchmark definition. There is also reciprocally an effect on the stock rail where the RCF prediction are locally higher with both constrained models. While the lateral constrained model shows very similar results to the simpler approach of having a solid profile for both switch and stock rail, this highlights the

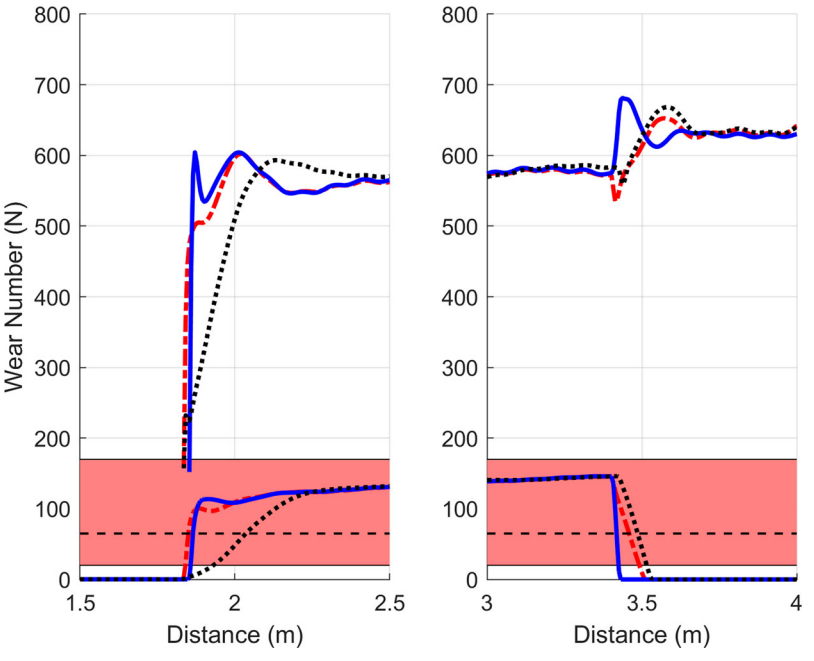

Figure 6. Run #2. Comparison of W/R Wear Index (T gamma) between the track model of the benchmark (black dotted), the laterally coupled dof (blue solid) and the solid connection (red semi-dashed) in VI-Rail. Left hand side focuses on the initial contact with the switch and right-hand side on the contact departure from the stock rail. The red rectangle shows the conditions leading to RCF, the black dash line being the highest risk [16]. Above the red rectangle, only wear occurs and increases with the Wear Index value.

fact that more accurate models of the switch panel including flexibility of rails would be required in order to assess the complete dynamic effects in this area of the switch toe, and more particularly where switch tip fatigue is of concern.

3.2. Effect of wheel shapes

In order to verify that the conclusions obtained so far on the rail separation are not affected by the type of wheel and rail used, a few additional simulations are carried out using wheels GB P8, and two worn GB P10 (equivalent to S1002), including one which is hollow worn. The results are plotted in Figure 7 based on the wear index output (T gamma) comparing both benchmark and constrained *dof* models. As can be seen, the different wheels lead to different initial flange contact position on the switch rail, as well as differing levels of wear magnitude. The hollow wheel Figure 7(c) shows the biggest change with a later contact with the switch rail and longer two-point contact. However it is obvious from these figures that only small differences in results are due to the separation of rails in the lateral direction, as compared to the effect of the wheel shape, and the same qualitative difference is observed on all these four cases.

3.3. Study of track models with a baseplate

Simulations of several possible track models with a baseplate are compared, starting from the simpler model (a) to the more complex one (d). The influence of the track models on

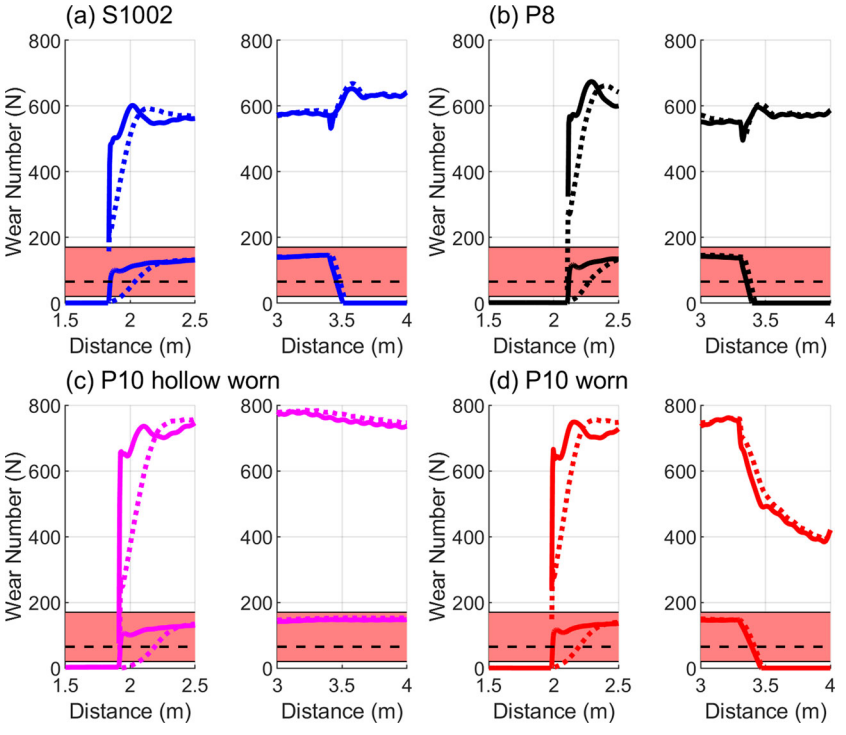

Figure 7. Run #2. Comparison of T gamma wear index in VI-Rail for four different wheel designs. Benchmark model (dash lines) and lateral constrained rails (solid lines).

the W/R forces and baseplate/switch rail forces is discussed in Section 3.4. In this section, the distribution of loads within the switch panel is studied for each of the four track models.

3.3.1. Model (a)

Model (a) is a three-layer model including a baseplate between the rails and the track (Figure 4(a)). As the switch rail rests on the baseplate, the compliance between the track and the switch rail is given by the baseplate pad.

Forces between the rails and the baseplate are plotted on the left side of Figure 8. Their pattern looks very similar to the W/R forces of previous models (Figure 5).

3.3.2. Model (b)

Model (b) is model (a) plus a connection between the rails. This connection is a unilateral normal contact operating in the undercut plane with an angle ϕ of 70° with no initial gap.

Forces between the rails and the baseplate are plotted on the right side of Figure 8. As sketched in Figure 1 or Figure 4(b), the vertical component of the normal force at the undercut plane tends to push the switch rail downward. Due to the inclined orientation of the undercut plane, the magnitude of the lateral projection of the normal force between the rails is higher than the vertical one. Even before the flanging contact, the magnitude of lateral forces is about +/−3 kN, which is not negligible. This is due to the high stiffness $k_{rb1,y}$ (1500 kN/mm see Table 1) of the connection between the baseplate and the switch rail. In comparison with the previous model (a), an additional oscillation at a frequency

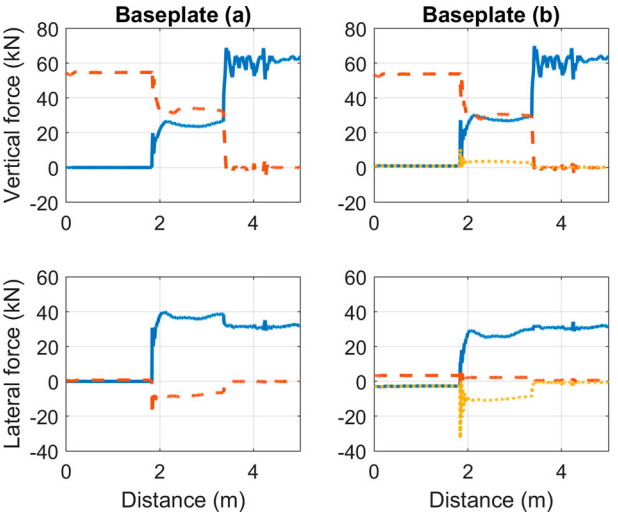

Figure 8. Run #2. VOCO results. Baseplate → stock rail (red dashed line) and baseplate → switch rail vertical and lateral forces (blue solid line) in models (a) and (b). Components of switch rail → stock rail normal forces (yellow dotted line) in model (b).

around 300 Hz is visible in the lateral component of the contact force at the undercut plane between the rails as a result of first flange contact with the switch rail. This oscillation is due to the transmission of the high impact force to both the rails through their stiff connection, while the relatively small rail mass is prone to vibrations. It is to be noted that the lumped mass co-running track model, might not represent sufficiently well the amount of structural damping that would be better represented by a discretely supported beam track model, i.e. transmitted some of the energy along the rails and track structure.

3.3.3. Model (c)

Model (c) is model (b) with a dry friction link in the lateral direction between the baseplate and the switch rail instead of a spring-damper. The steel on steel interface is supposed to be rough with a friction coefficient of 0.7 as this interface is generally subject to weathering and corrosion.

Forces in the switch panel are plotted on the left side of Figure 9. Coulomb's limit is also plotted. Due to Coulomb's law, the switch rail/baseplate lateral force is lower than in the previous model as there is saturation of the force and the switch rail would tend to slide and force against the stock rail. Consequently, stock rail/baseplate forces and stock rail/switch rail forces are higher. In comparison with the previous model (b), an additional peak in lateral forces is visible around 3.4 m at the transition zone from the stock rail to the switch rail. This corresponds to an increase of the switch rail/baseplate vertical force through the Coulomb's friction law. Higher short transient peaks are also found at the entrance of the switch at the interface between the switch rail and the baseplate. Because of the dry friction, the relatively high lateral forces of magnitude 3 kN visible in model (b) at the beginning of the switch have disappeared. Regarding this matter, model (c) seems more realistic than model (b).

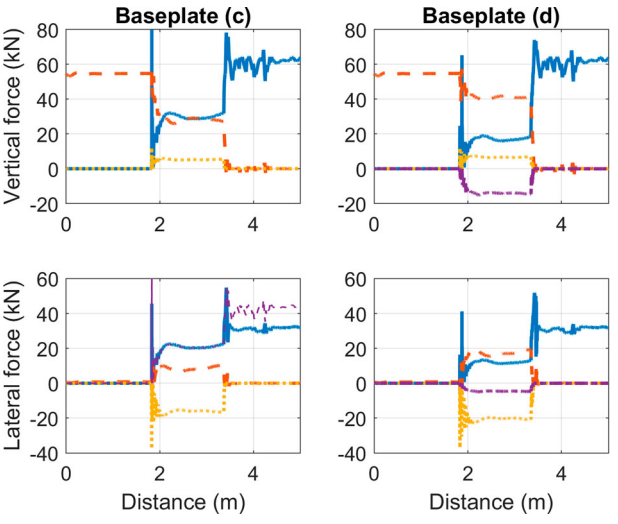

Figure 9. Run #2. VOCO results. Baseplate → stock rail (red dashed line) and baseplate → switch rail (blue solid line) vertical and lateral forces. Components of switch rail → stock rail normal forces (yellow dotted line) in models (c) and (d). Coulomb's limit on lateral baseplate → switch rail forces (thin magenta dashed line) in model (c). Components of switch rail → stock rail tangent forces (magenta dash-dotted line) in model (d).

3.3.4. Model (d)

Model (d) is model (c) plus dry friction in the tangent direction at the interface between both rails.

Forces in the switch panel are shown on the right side of Figure 9. Comparison with model (c) shows that the dry friction between the rails tends to mitigate peaks at the interface between the switch rail and the baseplate.

3.4. Summary of various configuration models

Figures 10 and 11 show the vertical and lateral forces on the switch rail, respectively, for all models and along the full length of the switch rail. Two-point contact occurs roughly between 1.8 and 3.4 m, after that the full wheel load is on the switch rail (stock rail load not plotted). The general observation is the benchmark model and the initial rigid coupling of both rails lead to one set of results, while the baseplate system leads to another group of results, essentially introducing higher frequency transient load at first contact, and higher transient loads while the wheel transfers fully onto the switch, especially in the lateral direction where coupling force elements are introduced.

Figures 12 and 13 show the vertical load for all cases, zoomed on the initial contact with the switch rail and zoomed on the contact departure from the stock rail, respectively.

The following observations are made on the first part (Figure 12):

- The benchmark definition is the most compliant of all, with a smoother build-up of the force on first contact with the leading wheel flange.

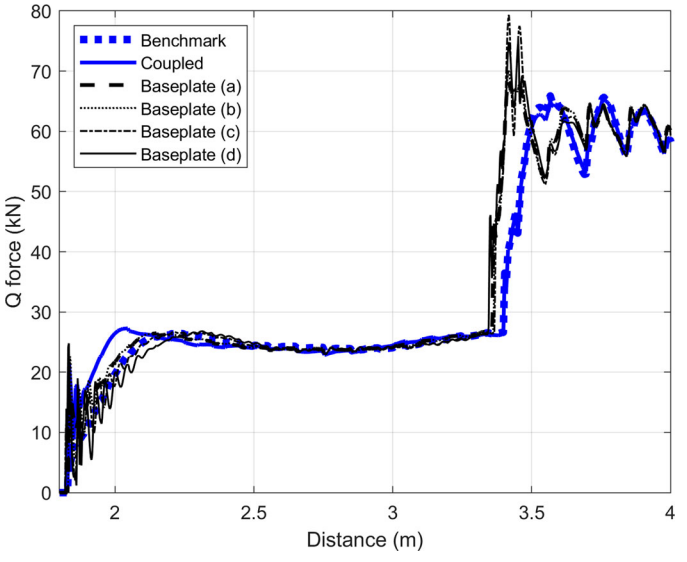

Figure 10. Vertical force on switch rail for all models.

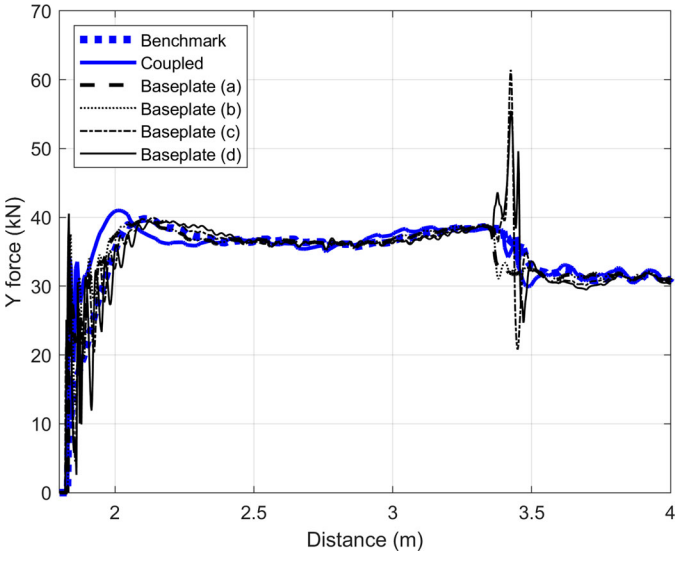

Figure 11. Lateral force on switch rail for all models.

- The introduction of a coupling between rails leads to a much steeper increase of force on the first contact, some oscillation of the load, and generally higher forces into the switch blade initially.
- The baseplate models follow the same trend and introduce further dynamics oscillation at higher frequency, which are exacerbated for models (c) and (d), due to the added Coulomb friction definition. However, the general rise of the force on the early part of the switch blade is not as high as the coupled model, and the baseplate can be seen to mitigate this.

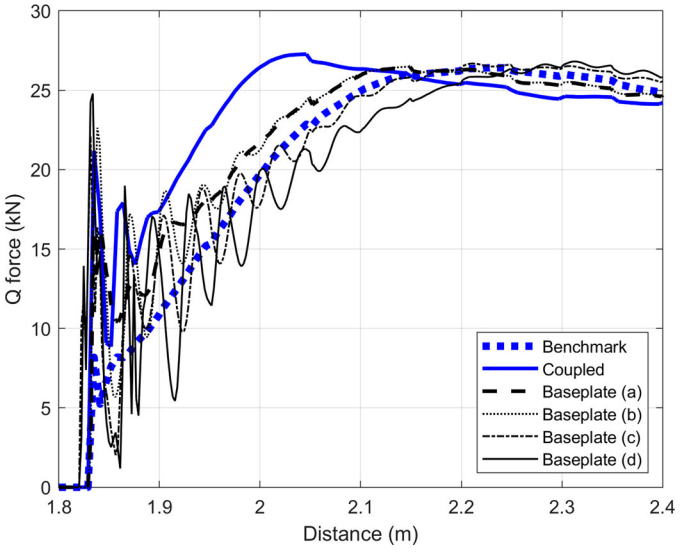

Figure 12. Vertical force on switch rail initial contact for all models.

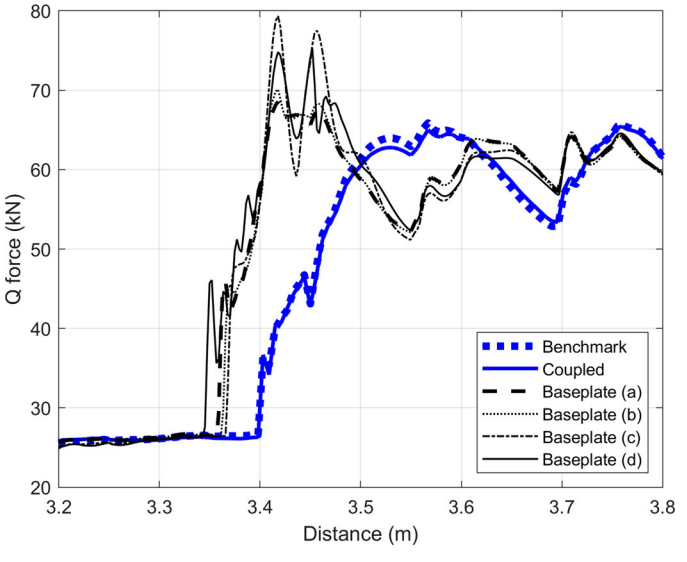

Figure 13. Vertical forces on switch rail after loss of contact with the stock rail for all models.

- Considering theses oscillations, it would be worthwhile to study the effect of different contact models with a damping term to accommodate the energy loss during the impact process [17].

The following observations are made on the later contact with the switch (Figure 13):

- Both the benchmark and coupled rail model give nearly identical results.

- The baseplate models show an earlier full transfer onto the switch rail, with a higher dynamic amplification factor.
- Baseplate models (c) and (d) show further increased dynamic loading at a high frequency on full load transfer, which is quickly damped out.

Interestingly, looking at the vertical and lateral forces exerted onto the switch rail by the baseplate at first contact with the switch rail (Figure 14), and ignoring high transient spikes

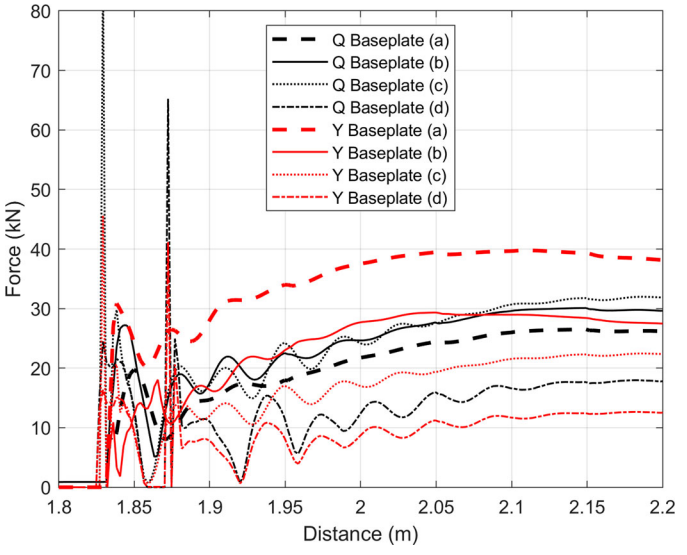

Figure 14. Forces (Q-black and Y-red) between the switch rail and the baseplate for all baseplate systems, on first contact with the switch rail.

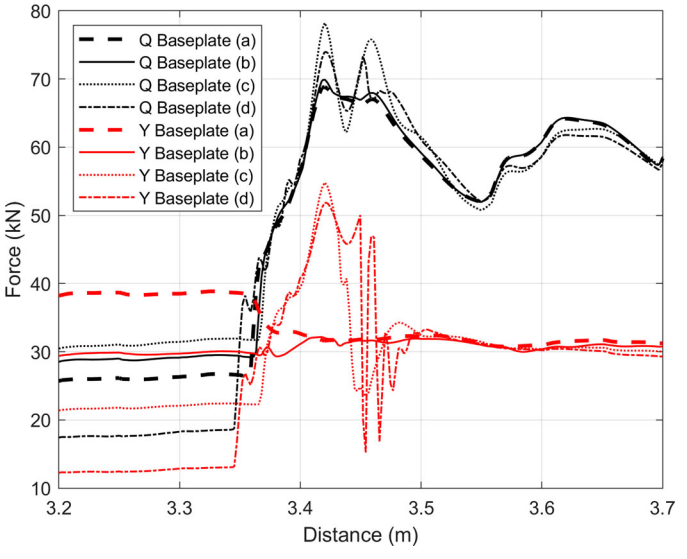

Figure 15. Forces (Q-black and Y-red) between the switch rail and the baseplate for all baseplate systems, on full load transfer to the switch rail.

from models (c) and (d), there is an obvious variation of loading onto the baseplate from each of the model variation, especially in the lateral direction (steady-state load between 12 and 40 kN). This modelling approach is therefore proving very interesting to estimate such loads that can be associated with a number of damage mechanism for baseplated switches, however, it is not possible from this study to say which option is the most realistic, as this would require further investigation and measurement, as well as better discretely support beam track models.

Figure 15 shows the vertical and lateral load onto the switch after full transfer. All baseplate models are showing the same trend following some initial high transient effect after the transfer, which is more prominent from the models (c) and (d) as shown from the overall contact forces.

4. Conclusions

This paper discusses the detailed implementation of the switch and stock rails relative movement whilst simulating vehicles running through switches in the diverging direction. The modelling approach proposed in the S&C benchmark is tested against the assumption that generally the switch rail rests against the stock rail and a very stiff connection between the two should be considered in the lateral direction. The results show that considering this rigid connection in the lateral direction leads to a sharper increase in flange contact loading on first contact as well as a more rapid full transition on the switch rail (departure from the stock rail). It was also shown that locally these higher transient effects can lead to increase wear prediction as well as slightly different contact energy prediction on the stock rail (a driver for RCF). However, apart from these variations observed at the start and end of the section where two-point contact occurs on both rails, the overall magnitude and global forces remain very similar in other areas. Results also indicate that only small differences in the contact conditions are due to the separation of rails in the lateral direction, as compared for example to other effects such as wheel shapes.

In a second part, this paper investigates further the detailed modelling of a baseplate system, to see if the relative motion between switch and stock rail can, and should be modelled considering unidirectional stiffness reaction and Coulomb friction interaction between the two rail parts. The results show that the introduction of the baseplate additional mass as well as the non-linear friction leads to increased dynamics effects especially on the first contact with the switch rail and on full departure from the stock rail (start and end of load sharing on both rails). These additional dynamic effects are mainly due to the vertical/lateral coupling of the contact in the undercut plane and to the dry friction. It is shown that the benchmark approach under-evaluates the dynamic aspects and potential damage at the switch toe on the first contact, while the coupled approach would tend to overestimate the forces and damage with respect to the baseplate system. As some of the configurations lead to oscillations of the wheel/rail forces, it would be worthwhile to consider contact models accounting for impact effects. The benefit of modelling the baseplate system allows to understand the respective load distribution between each of the rails and their support in the track structure which can be of interest for track design and maintenance. Also, this model taking into account the separation of rails is crucial as it could be used to study accidental derailment cases due to partial opening of switch blades. However, this work concludes that further investigation using more advanced flexible track models,

including beam approach for the rails would allow to fully study the complex behaviour of the system in this area and support any fatigue investigation on switch blades or track support as well as detailed derailment investigation studies able to consider cross effects of the axle loads of the vehicle.

Acknowledgements

The input from Xinggao Shu at TTCI is gratefully acknowledged for the several exchanges in conducting two complimentary papers on this topic. The support from the UK EPSRC project Track to the Future (grant agreement no. EP/M025276/1) and EU H2020 project In2Track2 (grant agreement No: 826255) is gratefully acknowledged by co-author Bezin.

Disclosure statement

No potential conflict of interest was reported by the author(s).

Funding

This work was supported by Engineering and Physical Sciences Research Council: [grant number EP/M025276/1]; H2020 European Institute of Innovation and Technology: [grant number 826255].

ORCID

Y. Bezin http://orcid.org/0000-0002-0599-8696

References

[1] Ma X, Wang P, Xu J, et al. Effect of the vertical relative motion of stock/switch rails on wheel rail contact mechanics in switch panel of railway turnout. Adv Mech Eng. 2018;10(7):1–13.
[2] Wang P, Ma X, Xu J, et al. Numerical investigation on effect of the relative motion of stock/switch rails on the load transfer distribution along the switch panel in high-speed railway turnout. Veh Syst Dyn. 2019;57(2):226–246.
[3] Bezin Y, Kostovasilis D, Sambo B. Relative movement of switch/stock rails and the wheel/rail interaction interface. In: Klomp M, Bruzelius F, Nielsen J, etal, editors. Advances in dynamics of vehicles on roads and tracks. IAVSD 2019. Lecture Notes in Mechanical Engineering. Gothenburg, Sweden: Springer; 2020. p. 367–375.
[4] Bezin Y, Kostovasilis D, Foan A. Enhanced S&C whole system analysis, design and virtual validation. In 2 Track EU Project (730841) Deliverable D2.2, Section 4.2.2 S&C Geometry & Rail Profile Optimisation. 2019.
[5] Bezin Y, Kostovasilis D, Neves S, et al. A broad approach to switch profiles optimisation using multibody dynamic simulation). In 4th International Conference on Railway Technology, 2018; Sitges, Spain.
[6] Bezin Y, Pålsson B. Multibody simulation benchmark for dynamic vehicle-track interaction in switches and crossings. Huddersfield: University of Huddersfield; 15 October 2019. doi:10.34696/s60x-ay18.
[7] Piotrowski J, Kik W. A simplified model of wheel/rail contact mechanics for non-Hertzian problems and its application in rail vehicle dynamic simulations. Veh Syst Dyn. 2008;46:27–48. doi: 10.1080/00423110701586444.
[8] Kalker JJ. A fast algorithm for the simplified Theory of rolling-contact. Veh Syst Dyn. 1982;11(1):1–13.
[9] Ayasse J, Chollet H. Determination of the wheel rail contact patch in semi-Hertzian conditions. Veh Syst Dyn. 2005;43:161–172. doi:10.1080/00423110412331327193.
[10] VI-Grade: VI-Rail Documentation. (2019).

[11] Bezin Y, Pålsson BA, Kik W, et al. Multibody simulation benchmark for dynamic vehicle-track interaction in switches and crossings: Results and method statements. 2020.
[12] Sebès M, Fan D, Qazi A, et al. VOCO statement of methods S&C benchmark. doi: XYZ. 2020.
[13] Magalhaes H, Marques F, Pombo, J, et al. Wheel-rail contact models in the presence of switches and crossings (to be submitted to VSD).
[14] Eickhoff B, Mazzola L, Bezin Y, et al. Track loading limits and cross acceptance of vehicle approvals. Proc Inst Mech Eng Part F J Rail Rapid Transit. 2015; 229(6):710–728.
[15] Chollet H, Sebès M, Maupu JL, et al. The VOCO multibody software in the context of real time simulation. Veh Syst Dyn. 2013;51(4):570–580.
[16] Burstow M. (2003). Whole life rail model application and development: Development of a rolling contact fatigue damage parameter. RSSB Report.
[17] Machado M, Moreira P, Flores P, et al. Compliant contact force models in multibody dynamics: evolution of the Hertz contact theory. Mech Mach Theory. 2012;53:99–121.